

Revisiting the magnetic responses of bilayer graphene from the perspective of the quantum distance

Chang-geun Oh,^{1,*} Jun-Won Rhim,^{2,3} and Bohm-Jung Yang^{4,5,6,†}

¹*Department of Applied Physics, The University of Tokyo, Tokyo 113-8656, Japan*

²*Department of Physics, Ajou University, Suwon 16499, Republic of Korea*

³*Research Center for Novel Epitaxial Quantum Architectures,*

Department of Physics, Seoul National University, Seoul 08826, Republic of Korea

⁴*Department of Physics and Astronomy, Seoul National University, Seoul 08826, Republic of Korea*

⁵*Center for Theoretical Physics (CTP), Seoul National University, Seoul 08826, Republic of Korea*

⁶*Institute of Applied Physics, Seoul National University, Seoul 08826, Republic of Korea*

We study the influence of the quantum geometry on the magnetic responses of quadratic band crossing semimetals. More explicitly, we examine the Landau levels, quantum Hall effect, and magnetic susceptibility of a general two-band Hamiltonian that has fixed isotropic quadratic band dispersion but with tunable quantum geometry, in which the interband coupling is fully characterized by the maximum quantum distance d_{\max} . By continuously tuning d_{\max} in the range of $0 \leq d_{\max} \leq 1$, we investigate how the magnetic properties of the free electron model with $d_{\max} = 0$ evolve into those of the bilayer graphene with $d_{\max} = 1$. We demonstrate that despite sharing the same energy dispersion $\epsilon(\mathbf{p}) = \pm \frac{p^2}{2m}$, the charge carriers in the free electron model and bilayer graphene exhibit entirely distinct Landau levels and quantum Hall responses due to the nontrivial quantum geometry of the wave functions.

I. INTRODUCTION

Graphene and its multilayer structures have garnered significant attention in various research fields, partly because of their unique carrier dynamics, sensitively dependent on the layer numbers [1–6]. One notable example is the distinct quantum Hall effect (QHE) in monolayer and bilayer graphenes [7–9]. In monolayer graphene with linear band touching points, the carriers with pseudo-relativistic dispersion result in the half-integral quantum Hall plateaus characterized by the unique Landau Level spectrum with the energy $\epsilon_N^{\text{single}} = \pm v_F \sqrt{2e\hbar B|N|}$, where v_F is the Fermi velocity [7–9], N is an integer, B is a magnetic field, and e , m are the electron's charge and mass, respectively. This unique behavior arises from the π Berry's phase of the Dirac points.

On the other hand, in Bernal stacked bilayer graphene, simply bilayer graphene hereafter, the charge carriers exhibit a parabolic dispersion $\epsilon(p) = \pm \frac{p^2}{2m}$ with the effective mass m , hosting the Landau levels $\epsilon_N^{\text{bilayer}} = \pm \hbar\omega \sqrt{N(N-1)}$. In bilayer graphene, the zero energy Hall plateau is absent, which is attributed to the 2π Berry phase around the quadratic band crossing point [9, 10]. It is noteworthy that although the parabolic band dispersion of the bilayer graphene is identical to that of the free electron gas, these two systems display entirely different Landau levels and QHEs. This indicates the importance of considering not only the band dispersion but also the geometry of wave functions to correctly describe the magnetic responses. The distinct Landau levels and QHEs of monolayer and bilayer graphenes are compared in Figure 1, in which we also plot the free electron gas Landau levels $\epsilon_N^{\text{conv}} = \pm \hbar\omega(N + \frac{1}{2})$ with the cyclotron frequency $\omega = eB/m$ [11, 12].

Recent studies have shown that the quantum distance is a central quantity characterizing the geometric properties of two-dimensional quadratic band touching systems, leading to intriguing phenomena such as anomalous Landau level spreading [13, 14] and the emergence of boundary modes in flat band systems [15, 16]. More explicitly, the Hilbert-Schmidt quantum distance, or simply quantum distance, in momentum space is defined as

$$d_{\text{HS},n}^2(\mathbf{k}, \mathbf{k}') = 1 - |\langle \psi_{n,\mathbf{k}} | \psi_{n,\mathbf{k}'} \rangle|^2, \quad (1)$$

where n is a band index and $\psi_{n,\mathbf{k}}$ is the Bloch eigenstate of the n -th band with crystal momentum \mathbf{k} . In particular, it was shown that the maximum quantum distance, denoted as d_{\max} , determines various geometric properties of the quadratic band crossing semimetals, including the Berry's phase [17, 18]. In terms of d_{\max} , the geometry of bilayer graphene is characterized by $d_{\max} = 1$, while the free electron with a quadratic band crossing is described by $d_{\max} = 0$, indicating geometric triviality. Although these two systems have two distinct d_{\max} values, to properly understand the role of the interband coupling in their distinct magnetic responses, one can design a model Hamiltonian that has fixed isotropic quadratic band dispersion $\epsilon(p) = \pm \frac{p^2}{2m}$ but with tunable quantum geometry.

In this paper, we examine the Landau levels, QHE, and magnetic response functions of the geometrically generalized model. By thoroughly examining them, we illustrate the nontrivial role of the interband coupling measured by d_{\max} in magnetic responses of quadratic band crossing semimetals.

The rest of the paper is organized as follows. In Sec. II, we construct a model Hamiltonian for isotropic quadratic band touching semimetals, where the band dispersion remains $\pm p^2/(2m)$ while the geometry of wave functions is tunable. In Sec. III, we analyze the Landau levels of the model and examines the role of wave function geometry. In Sec. IV, we investigate the evolution of QHE between free electron gas and bilayer graphene. In Sec. V, we further explore the influence of wave function geometry on magnetic response functions

* cg.oh.0404@gmail.com

† bjang@snu.ac.kr

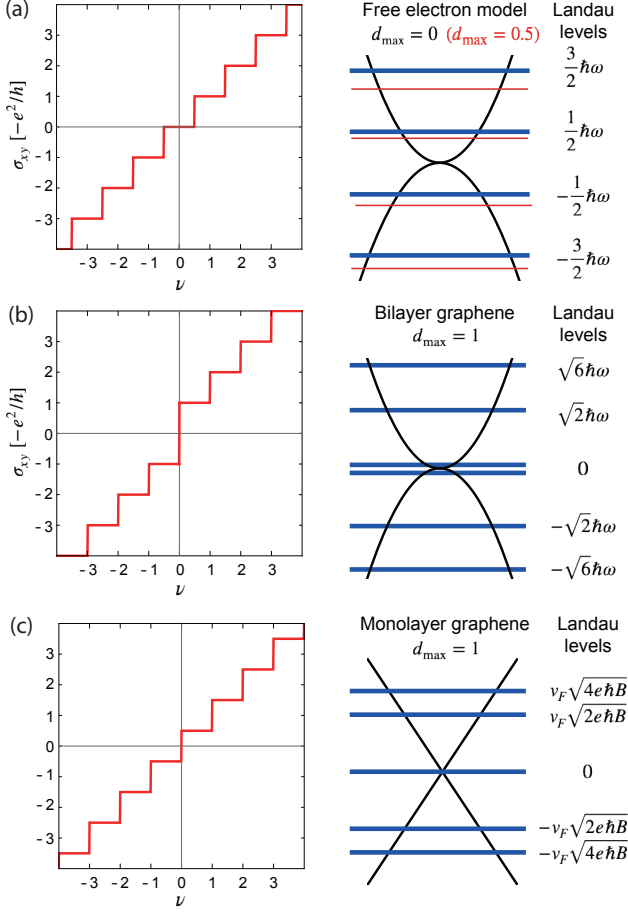


FIG. 1. Schematics of the representative integer quantum Hall effect (left) and the corresponding Landau level spectrum (right) for (a) free electron model, characterized by geometric triviality ($d_{\max} = 0$), (b) bilayer graphene, featuring nontrivial geometry with $d_{\max} = 1$, and (c) monolayer graphene, also exhibiting geometric nontriviality with $d_{\max} = 1$. The red horizontal lines in (a) represent the Landau levels of a quadratic band crossing in Eq. (3) featuring nontrivial quantum geometry with $d_{\max} = 0.5$.

using the Roth-Gaou-Niu relation [19–21]. Our concluding remarks can be found in Sec. VI. Appendixes contains the detailed calculations of Landau levels and a lattice model analysis.

II. MODEL

Let us construct a general Hamiltonian whose energy eigenvalues are given by

$$\epsilon_{\pm}(\mathbf{k}) = \pm \frac{1}{2}(k_x^2 + k_y^2). \quad (2)$$

Explicitly, we consider the Hamiltonian

$$\mathcal{H}_0(\mathbf{k}) = \sum_{\alpha} h_{\alpha}(\mathbf{k})\sigma_{\alpha}, \quad (3)$$

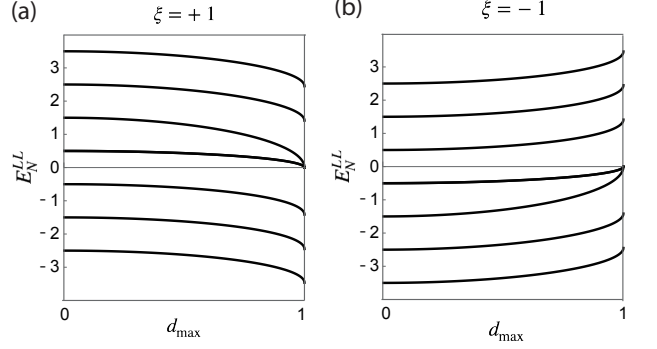


FIG. 2. The evolution of the Landau levels E_N^{LL} as a function of the maximum quantum distance d_{\max} for (a) $\xi = +1$ and (b) $\xi = -1$, respectively, with $\hbar = \omega = 1$.

where σ_{α} represents an identity ($\alpha = 0$) and Pauli matrices ($\alpha = x, y, z$), respectively. $h_{x,y,z}(\mathbf{k})$ are real quadratic functions given by $h_z(\mathbf{k}) = -d\sqrt{1-d^2}k_y^2$, $h_y(\mathbf{k}) = dk_x k_y$, $h_x(\mathbf{k}) = k_x^2/2 + (1-2d^2)k_y^2/2$, and $h_0(\mathbf{k}) = 0$. Here, the parameter d is defined as $d = \xi d_{\max}$ in which $\xi = \pm 1$, and d_{\max} is the maximum value of the quantum distance $d_{\text{HS},n}(\mathbf{k}, \mathbf{k}')$ between all the possible pairs of wave functions at \mathbf{k} and \mathbf{k}' with the given band index $n = 1, 2$. The energy eigenvalues of $\mathcal{H}_0(\mathbf{k})$ remain unchanged from Eq. (2) regardless of the value of d within the range $-1 \leq d \leq 1$. When $d_{\max} = 1$, the Hamiltonian in Eq. (3) corresponds to the low energy Hamiltonian of the Bernal stacked bilayer graphene [22, 23], and $\xi = \pm 1$ is related to the valley index. The parameters d_{\max} and ξ determine the Berry phase Φ_B [17] and quantum geometric tensor g_{ij}^n given by $g_{ij}^n = \langle \partial_{k_i} u_n(\mathbf{k}) | \partial_{k_j} u_n(\mathbf{k}) \rangle - \langle \partial_{k_i} u_n(\mathbf{k}) | u_n(\mathbf{k}) \rangle \langle u_n(\mathbf{k}) | \partial_{k_j} u_n(\mathbf{k}) \rangle$, where $u_n(\mathbf{k})$ is the n -th Bloch wave function [24]. Explicitly, for $\mathcal{H}_0(\mathbf{k})$, the Berry phase and components of the quantum geometric tensor are given by

$$\Phi_B = -2\pi\xi\sqrt{1-d_{\max}^2} \pmod{2\pi}, \quad (4)$$

$$g_{xx}^n(\mathbf{k}) = d_{\max}^2 \frac{k_y^2}{k^4}, \quad g_{yy}^n(\mathbf{k}) = d_{\max}^2 \frac{k_x^2}{k^4},$$

$$g_{xy}^n(\mathbf{k}) = g_{yx}^n(\mathbf{k}) = -d_{\max}^2 \frac{k_x k_y}{k^4}. \quad (5)$$

We note that more general quadratic band touching Hamiltonians, which exhibit anisotropic energy dispersions, require other geometric quantities to describe all possible interband coupling terms [18]. However, when the system has rotational symmetry, a single geometric parameter d_{\max} suffices to fully characterize the quantum geometry [17, 18].

III. LANDAU LEVELS

To understand the evolution of the Landau levels between ϵ_N^{conv} [Fig. 1(a)] and $\epsilon_N^{\text{bilayer}}$ [Fig. 1(b)], we introduce a magnetic field B to the Hamiltonian in Eq. (3). We replace the momentum by ladder operators as $k_x \rightarrow (a + a^\dagger)/(\sqrt{2}l_B)$ and

$k_y \rightarrow i(a - a^\dagger)/(\sqrt{2}l_B)$, where $l_B = \sqrt{\hbar/eB}$ is the magnetic length, and $a(a^\dagger)$ is the annihilation (creation) operator. To ensure the Hamiltonian's hermiticity, we perform symmetrization: $k_x k_y = (k_x k_y + k_y k_x)/2 = i(a^2 - (a^\dagger)^2)/(2l_B^2)$.

Solving the transformed Hamiltonian yields the Landau levels (see Appendix for details):

$$\begin{aligned} E_0^{LL}(d_{\max}, \xi) &= \frac{\xi}{2} \hbar \omega \sqrt{1 - d_{\max}^2}, \\ E_1^{LL}(d_{\max}, \xi) &= \frac{3\xi}{2} \hbar \omega \sqrt{1 - d_{\max}^2}, \\ E_N^{LL}(d_{\max}, \xi) &= \xi \hbar \omega \left(\sqrt{1 - d_{\max}^2} \right. \\ &\quad \left. + \frac{\text{sgn}(N)}{2} \sqrt{(2|N| - 1)^2 - d_{\max}^2} \right), \end{aligned} \quad (6)$$

where $N = \pm 2, \pm 3, \dots$ and $\text{sgn}(N)$ represents the sign of N .

In Figure 2, the d_{\max} -dependence of Landau levels is depicted. When $d_{\max} = 0$, the Landau levels E_N^{LL} are equivalent to ϵ_N^{conv} but start to deviate from ϵ_N^{conv} as d_{\max} increases. When d_{\max} reaches one, they become $\epsilon_N^{\text{bilayer}}$. The degeneracy of Landau levels between $E_0^{LL}(d_{\max} = 1)$ and $E_1^{LL}(d_{\max} = 1)$ leads to the absence of a zero energy plateau in QHE as described in Section IV. Since such degeneracy of Landau levels occurs only when $d_{\max} = 1$, the absence of the zero energy plateau cannot be observed if $d_{\max} \neq 1$.

One can verify that the degeneracy at $d_{\max} = 1$ exists for both $\xi = \pm 1$. However, depending on ξ , the origin of zero Landau levels is different. For $\xi = +1$, the two zero energy levels come from the upper band, while for $\xi = -1$, the two zero energy levels come from the lower band. In a previous work [25], this ξ -dependence of zero energy Landau levels was demonstrated by creating a gap between two bands in bilayer graphene. Here, on the other hand, we verify that the ξ -dependence of zero energy Landau levels by continuously varying the quantum distance.

Furthermore, when $d_{\max} = 1$ or $d_{\max} = 0$, the Landau levels are symmetric with respect to $E = 0$, as shown in Figs. 2(a) and (b). This result arises from chiral symmetry, represented by the operator σ_z , which satisfies $\sigma_z H_0(\mathbf{k}) \sigma_z = -H_0(\mathbf{k})$, exclusively when $d_{\max} = 1$ or $d_{\max} = 0$. This symmetry holds even in the presence of a magnetic field (See Appendix). In fact, the chiral symmetry is crucial for the degeneracy observed at $d_{\max} = 1$. To confirm this idea, we introduce a perturbation $H_{\text{pert}} = \delta k^2 \sigma_0$ that breaks the chiral symmetry, and subsequently calculate the resulting Landau levels. With this perturbation, the zeroth and first Landau levels for $d_{\max} = 1$ shift to $E_0^{LL} = \frac{\xi}{2} \hbar \omega \delta$ and $E_1^{LL} = \frac{3\xi}{2} \hbar \omega \delta$, respectively, thereby lifting the degeneracy. This demonstrates that the presence of the zero energy plateau necessitates chiral symmetry as well as $d_{\max} = 1$.

In addition, when the Hamiltonian possesses chiral symmetry, one can define a winding number (W):

$$W \equiv \int_C \frac{d\mathbf{k}}{2\pi} \left[\frac{h_x}{|\mathbf{h}|} \nabla \left(\frac{h_y}{|\mathbf{h}|} \right) - \frac{h_y}{|\mathbf{h}|} \nabla \left(\frac{h_x}{|\mathbf{h}|} \right) \right]. \quad (7)$$

Explicitly, for $d_{\max} = 0$ and $d_{\max} = 1$, we obtain

$$\begin{aligned} W &= 0 \quad \text{for } d_{\max} = 0 \text{ and } \xi = \pm 1, \\ W &= +2 \quad \text{for } d_{\max} = 1 \text{ and } \xi = +1, \\ W &= -2 \quad \text{for } d_{\max} = 1 \text{ and } \xi = -1. \end{aligned} \quad (8)$$

This indicates that the presence of the zero energy plateau is contingent upon chiral symmetry with a winding number of two.

For $0 < d_{\max} < 1$, the chiral symmetry is broken because the Hamiltonian in Eq. (3) has nonzero h_x , h_y and h_z , simultaneously. Consequently, the Landau levels are no longer symmetric with respect to $E = 0$. However, one can still find the symmetry between $\xi = +1$ and $\xi = -1$ cases in which the Landau levels have the opposite signs, as shown in Eq. (6), Figs. 2(a) and (b). For $|N| \gg 1$, this can be understood using the semiclassical results given by [20]

$$E_N = \hbar \omega \left(N + \frac{1}{2} - \frac{\Phi_B}{2\pi} \right), \quad (9)$$

where Φ_B is Berry phase. For both $\xi = \pm 1$ cases with $|N| \gg 1$, the Landau levels in Eq. (6) are identical to those in Eq. (9). Depending on ξ , the sign of Φ_B changes oppositely, as shown in Eq. (4), explaining the symmetric structure of the Landau levels between $\xi = +1$ and $\xi = -1$ cases. Interestingly, this symmetric structure persists even for low N as explicitly shown in Eq. (6).

IV. QUANTUM HALL EFFECT

The dependence of the Landau levels on d_{\max} significantly influences the QHE. Here, we focus on the case $\xi = +1$; the results for $\xi = -1$ can be obtained by reversing the sign of the energies for $\xi = 1$ as shown in Fig. 2. To understand the influence of d_{\max} on QHE, it is more insightful to examine the magnetic field dependence of Hall conductivity or Hall resistivity rather than the filling factor dependence of Hall conductivity. This is because the continuous variation from $d_{\max} = 0$ to $d_{\max} = 1$ is not apparent in the latter case; instead, a sudden change is observed at $d_{\max} = 1$ due to the zero energy degeneracy. Therefore, we analyze the magnetic field dependence of QHE by varying d_{\max} when the electron density is fixed.

Figure 3(a) shows the magnetic field dependence of the Landau levels in Eq. (6). As the magnetic field increases, the topmost occupied level changes when the filling factor ν reaches integer values. At these points, E_F transitions from E_ν^{LL} to $E_{\nu-1}^{LL}$. Figure 3(b) shows the magnetic field dependence of the Fermi energy $E_F(B)$, referred to as Shubnikov-de Hass oscillation, for various values of $d_{\max} = 0, 0.5, 0.8$ and 1. Increasing d_{\max} shifts the magnetic field $B_{\nu=i}$ where the transition occurs with an integer i . Furthermore, the slope of the Fermi energy at $B_{\nu=i}$, defined as

$$m_i := \lim_{\delta \rightarrow 0^+} \frac{E_F(B_{\nu=i} + 2\delta) - E_F(B_{\nu=i} + \delta)}{\delta}, \quad (10)$$

decreases with higher values of d_{\max} . Specifically,

$$m_1 = \frac{\hbar e}{2m} \sqrt{1 - d_{\max}^2}, \quad (11)$$

$$m_2 = \frac{3\hbar e}{2m} \sqrt{1 - d_{\max}^2}. \quad (12)$$

More generally, $m_i = E_{i-1}^{LL}/B$. The decrease in the slopes m_1 and m_2 with increasing d_{\max} causes B_1 , where the E_F transitions from E_1^{LL} to E_0^{LL} , to increase. When d_{\max} reaches one, these slopes approach zero, making B_1 infinite. This implies that the first Landau level E_1^{LL} is always occupied when $E_F^{(0)} > 0$ where $E_F^{(0)}$ is the Fermi level at zero magnetic field.

To consider Hall plateaus, we assume the disorder induced Landau level broadening as schematically illustrated in Figure 3(e) where delocalized electrons exist in the middle of each level while the rest of the states are localized. Figure 3(c) shows the magnetic field dependence of Hall resistivity for $d_{\max} = 0, 0.5, 0.8$ and 1 . The Hall resistivity ρ_{xy} is quantized as $\rho_{xy} = -h/(ne^2)$ with a natural number n . Similar to the oscillating E_F , the magnetic field at which ρ_{xy} jumps strongly depends on d_{\max} . Increasing d_{\max} extends the length of $n = 1$ plateau and shifts the magnetic field B^* where the transition from $n = 1$ plateau to $n = 0$ plateau occurs. Figure 3(d) shows the d_{\max} dependence of B^* . When $d_{\max} = 1$, B^* becomes infinity, indicating that the $n = 0$ plateau does not exist.

Furthermore, in Fig. 3(c), one can observe that the jump between $n = 1$ and $n = 2$ plateaus occurs at higher magnetic fields as d_{\max} increases when $0 \leq d_{\max} < 1$. However, when $d_{\max} = 1$, this jump suddenly occurs at a relatively lower magnetic field. This phenomenon originates from the chiral symmetry and the degeneracy between the zeroth and first Landau levels in Eq. (6).

More explicitly, the Hall resistivity changes when the Fermi energy passes the delocalized state, as shown in Fig. 3(e). For $d_{\max} < 1$, the transition between the $n = 1$ and $n = 2$ plateaus occurs when $E_F^{(0)} = E_1^{LL}$. Since $E_1^{LL}(d_{\max}) = \frac{3\hbar e}{2m} B \sqrt{1 - d_{\max}^2}$, the jump requires a higher B as d_{\max} increases. On the other hand, at $d_{\max} = 1$, the transition between the $n = 1$ and $n = 2$ plateaus happens when $E_F^{(0)} = E_2^{LL} = \frac{\hbar e}{m} \sqrt{2} B$. This is because filling E_0^{LL} and E_1^{LL} corresponds to the jump between $n = -1$ and $n = +1$ plateaus due to chiral symmetry. Note that the system is electrically neutral when both E_0^{LL} and E_1^{LL} are half-filled. Therefore, the transition between $n = 1$ and $n = 2$ plateaus occurs when $E_F^{(0)} = E_2^{LL}(d_{\max} = 1)$, while for $d_{\max} < 1$ it occurs when $E_F^{(0)} = E_1^{LL}$ [Fig. 3(e)]. Consequently, the jump between $n = 1$ and $n = 2$ plateaus for $d_{\max} = 1$ does not follow the trend observed when $d_{\max} < 1$.

V. MAGNETIC RESPONSE FUNCTIONS

Magnetic response functions also exhibit strong dependence on d_{\max} . We explore how d_{\max} influences magnetic response functions by utilizing the Roth-Gaou-Niu relation

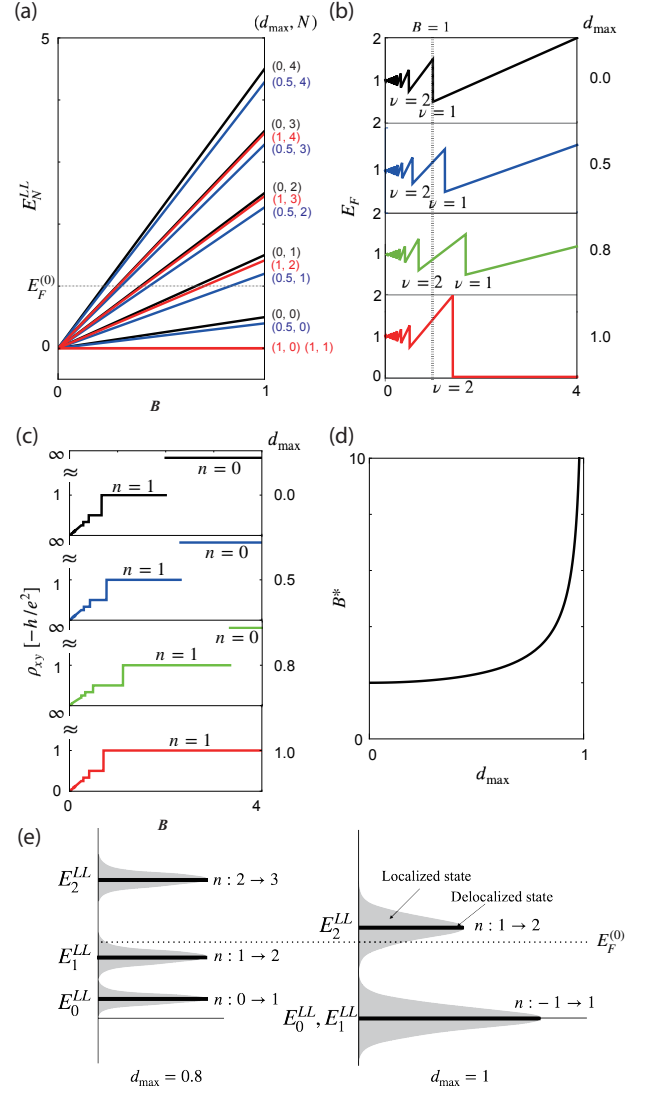


FIG. 3. (a) The magnetic field B dependence of Landau levels E_N^{LL} for $d_{\max} = 0, 0.5$ and 1 with $\hbar = e = 1$ and $\xi = +1$. (b) B dependence of the Fermi level E_F for $d_{\max} = 0, 0.5, 0.8$ and 1 . (c) B dependence of the Hall resistivity ρ_{xy} for $d_{\max} = 0, 0.5, 0.8$ and 1 . The black, blue, green and red lines in (a-c) represent $d_{\max} = 0, 0.5, 0.8$ and 1 , respectively. (d) The maximum quantum distance d_{\max} dependence of the magnetic field B^* , where the jump from $n = 1$ to $n = 0$ in ρ_{xy} occurs. Here, we set the Fermi energy at zero magnetic field as $E_F^{(0)} = 1$. (e) Schematics of Landau levels in disordered system for $d_{\max} = 0.8$ and 1 . The grey and black areas represent localized and delocalized states, respectively. $n : i \rightarrow i + 1$ ($i = 0, 1$) next to delocalized states indicate the corresponding jump in ρ_{xy} . Here, we consider the situation where Hall resistivity is on the $n = 2$ ($n = 1$) plateau for $d_{\max} = 0.8$ ($d_{\max} = 1$).

[19–21] given by

$$(N - \frac{1}{2}) \frac{eB}{h} = N_0(\epsilon_F) + BM'_0(\epsilon_F) + \frac{B^2}{2} \chi'_0(\epsilon_F) + O(B^3), \quad (13)$$

where $N_0(\epsilon_F)$ is the zero-field integrated density of states at the Fermi energy ϵ_F (i.e., $N'_0 = \partial_\epsilon N_0$ is the density of states), $M_0(\epsilon_F)$ is the spontaneous magnetization, and $\chi_0(\epsilon_F)$ is the magnetic susceptibility. Here, the prime denotes the derivative with respect to the energy: $M'_0 = \partial_\epsilon M_0$, $\chi'_0 = \partial_\epsilon \chi_0(\epsilon)$. These quantities, which depend on the Fermi energy ϵ_F , are evaluated at zero temperature and in the limit of zero magnetic field. Below, we adopt units where $\hbar = 1$ and the flux quantum $\phi_0 = h/e = 1$.

By applying the results in Eq. (6) to Eq. (13), we obtain the following expressions [26]

$$N_0(\epsilon_F) = \frac{\epsilon_F}{2\pi}, \quad (14)$$

$$M'_0(\epsilon_F) = \frac{\Phi_B(d_{\max})}{2\pi}, \quad (15)$$

$$\chi'_0(\epsilon_F) = d_{\max}^2 \frac{\pi}{2\epsilon_F}. \quad (16)$$

We note that the integrated density of states $N_0(\epsilon_F)$ solely depends on ϵ_F independent of d_{\max} because d_{\max} does not contribute to the energy dispersion.

The fact that the derivative of M_0 is proportional to the Berry phase indicates that the average of the orbital magnetic moment over the Fermi surface vanishes, i.e., $\langle \mathcal{M} \rangle_{\epsilon_F} = 0$. This is because, according to the modern theory of magnetization [21, 27, 28], differentiating the magnetization with respect to the chemical potential gives

$$M'_0(\epsilon_F) = \langle \mathcal{M} \rangle_{\epsilon_F} N'_0(\epsilon_F) + \frac{\Phi_B(d_{\max})}{2\pi}, \quad (17)$$

where $\langle \mathcal{M} \rangle_{\epsilon_F}$ represents the average of the orbital magnetic moment over the Fermi surface. Indeed, for a two-band model with electron-hole symmetry, the orbital magnetic moment is directly related to the Berry curvature: $\mathcal{M}(\mathbf{k}) = \frac{e}{\hbar} \epsilon_+(\mathbf{k}) \Omega(\mathbf{k})$, where Ω is the Berry curvature [29, 30]. In a quadratic band touching semimetal, the Berry curvature at finite \mathbf{k} is always zero while the Berry phase $\Phi_B(d_{\max})$ can be finite [17]. Therefore, the average of the orbital magnetic moment over the Fermi surface vanishes, and $M'_0(\epsilon_F) = \frac{\Phi_B(d_{\max})}{2\pi}$.

The result for the derivative of the susceptibility agrees with the known results for free electron model and bilayer graphene when $d_{\max} = 0$ and $d_{\max} = 1$, respectively [21, 22, 31].

Considering the form of the susceptibility in the free electron model and bilayer graphene as well as Eq. (16) [32], we propose the following expression for the susceptibility:

$$\chi_0(\epsilon_F) = \frac{\pi}{2} \left(\frac{1}{3} + d_{\max}^2 \ln \frac{|\epsilon_F|}{t} \right), \quad (18)$$

where t is a constant. For bilayer graphene, the constant t is related to interlayer hopping [22, 31]. One can verify that the derivative of the above equation gives Eq. (16).

VI. CONCLUSION

To summarize, we have studied the influence of d_{\max} on Landau levels, the QHE, and magnetic response functions of isotropic quadratic band-touching systems. Despite sharing the same energy dispersion, distinct wave function geometry, characterized by different d_{\max} , gives rise to markedly different Landau levels, QHE, and magnetic response functions. Our finding underscores the significance of quantum geometry of wavefunctions on the magnetic properties of electronic systems. Considering the growing interest in the physical responses induced by the quantum geometry, revealing the relation between physical responses and geometry in more general multi-band semimetal systems is an important direction for future study.

ACKNOWLEDGMENTS

We thank Haruki Watanabe, Mikito Koshino and Junseo Jung for the useful discussions. C-g.O. was supported by Q-STEP, WINGS Program, the University of Tokyo. J.W.R. was supported by the National Research Foundation of Korea (NRF) Grant funded by the Korean government (MSIT) (Grant no. 2021R1A2C1010572 and 2021R1A5A1032996 and 2022M3H3A106307411) and the Ministry of Education (Grant no. RS-2023-00285390). B.-J.Y. was supported by Samsung Science and Technology Foundation under Project No. SSTF-BA2002-06, and National Research Foundation of Korea (NRF) grants funded by the government of Korea (MSIT) (Grants No. NRF-2021R1A5A1032996).

-
- [1] T. Ando and T. Nakanishi, Impurity scattering in carbon nanotubes—absence of back scattering—, *Journal of the Physical Society of Japan* **67**, 1704 (1998).
 - [2] T. Ando, Theory of electronic states and transport in carbon nanotubes, *Journal of the Physical Society of Japan* **74**, 777 (2005).
 - [3] M. I. Katsnelson, K. S. Novoselov, and A. K. Geim, Chiral tunnelling and the Klein paradox in graphene, *Nature physics* **2**, 620 (2006).
 - [4] A. F. Young and P. Kim, Quantum interference and Klein tunnelling in graphene heterojunctions, *Nature Physics* **5**, 222 (2009).
 - [5] E. McCann, K. Kechedzhi, V. I. Fal'ko, H. Suzuura, T. Ando, and B. Altshuler, Weak-localization magnetoresistance and valley symmetry in graphene, *Physical review letters* **97**, 146805 (2006).
 - [6] F. Tikhonchenko, A. Kozikov, A. Savchenko, and R. Gorbachev, Transition between electron localization and antilocalization in graphene, *Physical Review Letters* **103**, 226801 (2009).
 - [7] K. S. Novoselov, A. K. Geim, S. V. Morozov, D. Jiang, M. I. Katsnelson, I. V. Grigorieva, S. Dubonos, Firsov, and A. A. Two-dimensional gas of massless Dirac fermions in graphene, *nature*

- 438**, 197 (2005).
- [8] Y. Zhang, Y.-W. Tan, H. L. Stormer, and P. Kim, Experimental observation of the quantum hall effect and berry's phase in graphene, *nature* **438**, 201 (2005).
- [9] K. S. Novoselov, E. McCann, S. Morozov, V. I. Fal'ko, M. Katsnelson, U. Zeitler, D. Jiang, F. Schedin, and A. Geim, Unconventional quantum hall effect and berry's phase of 2π in bilayer graphene, *Nature physics* **2**, 177 (2006).
- [10] V. I. Fal'ko, Electronic properties and the quantum hall effect in bilayer graphene, *Philosophical Transactions of the Royal Society A: Mathematical, Physical and Engineering Sciences* **366**, 205 (2008).
- [11] S. Girvin and R. Prange, *The quantum hall effect*, (1987).
- [12] A. H. MacDonald and A. H. MacDonald, *Quantum Hall effect: a perspective* (Springer, 1989).
- [13] J.-W. Rhim, K. Kim, and B.-J. Yang, Quantum distance and anomalous landau levels of flat bands, *Nature* **584**, 59 (2020).
- [14] J.-W. Rhim and B.-J. Yang, Singular flat bands, *Advances in Physics: X* **6**, 1901606 (2021).
- [15] C.-g. Oh, D. Cho, S. Y. Park, and J.-W. Rhim, Bulk-interface correspondence from quantum distance in flat band systems, *Communications Physics* **5**, 320 (2022).
- [16] H. Kim, C.-g. Oh, and J.-W. Rhim, General construction scheme for geometrically nontrivial flat band models, *arXiv preprint arXiv:2305.00448* (2023).
- [17] Y. Hwang, J. Jung, J.-W. Rhim, and B.-J. Yang, Wave-function geometry of band crossing points in two dimensions, *Physical Review B* **103**, L241102 (2021).
- [18] J. Jung, H. Lim, and B.-J. Yang, Quantum geometry and landau levels of quadratic band crossings, *Physical Review B* **109**, 035134 (2024).
- [19] Y. Gao and Q. Niu, Zero-field magnetic response functions in landau levels, *Proceedings of the National Academy of Sciences* **114**, 7295 (2017).
- [20] L. M. Roth, Semiclassical theory of magnetic energy levels and magnetic susceptibility of bloch electrons, *Physical Review* **145**, 434 (1966).
- [21] J.-N. Fuchs, F. Piéchon, and G. Montambaux, Landau levels, response functions and magnetic oscillations from a generalized onsager relation, *SciPost Physics* **4**, 024 (2018).
- [22] M. Koshino and T. Ando, Orbital diamagnetism in multilayer graphenes: Systematic study with the effective mass approximation, *Physical Review B* **76**, 085425 (2007).
- [23] E. McCann and M. Koshino, The electronic properties of bilayer graphene, *Reports on Progress in physics* **76**, 056503 (2013).
- [24] J. Provost and G. Vallee, Riemannian structure on manifolds of quantum states, *Communications in Mathematical Physics* **76**, 289 (1980).
- [25] M. Koshino and T. Ando, Anomalous orbital magnetism in dirac-electron systems: role of pseudospin paramagnetism, *Physical Review B* **81**, 195431 (2010).
- [26] Solve $E_N^{LJ} = \epsilon_F$ for N , then we get the results.
- [27] D. Xiao, M.-C. Chang, and Q. Niu, Berry phase effects on electronic properties, *Reviews of modern physics* **82**, 1959 (2010).
- [28] T. Thonhauser, Theory of orbital magnetization in solids, *International Journal of Modern Physics B* **25**, 1429 (2011).
- [29] D. Xiao, W. Yao, and Q. Niu, Valley-contrasting physics in graphene: magnetic moment and topological transport, *Physical review letters* **99**, 236809 (2007).
- [30] J. Fuchs, F. Piéchon, M. Goerbig, and G. Montambaux, Topological berry phase and semiclassical quantization of cyclotron orbits for two dimensional electrons in coupled band models, *The European Physical Journal B* **77**, 351 (2010).
- [31] S. Safran, Stage dependence of magnetic susceptibility of intercalated graphite, *Physical Review B* **30**, 421 (1984).
- [32] The susceptibility is given $\chi_0(\epsilon_F) = \frac{\pi}{6}$ for free electrons, $\chi_0(\epsilon_F) = \frac{\pi}{2}(\frac{1}{3} + \ln \frac{|\epsilon_F|}{t})$ for bilayer graphene[21, 22, 31], and $\chi'_0(\epsilon_F) = d_{\max}^2 \frac{\pi}{2\epsilon_F}$.

Appendix A: Landau levels of the continuum model

The continuum Hamiltonian is given by

$$\mathcal{H}_0(\mathbf{k}) = \sum_{\alpha} h_{\alpha}(\mathbf{k})\sigma_{\alpha}, \quad (\text{A1})$$

where σ_{α} represents an identity ($\alpha = 0$) and Pauli matrices ($\alpha = x, y, z$). Here, $h_{\alpha}(\mathbf{k})$ is a real quadratic function: $h_x(\mathbf{k}) = d\sqrt{1-d^2}k_y^2$, $h_y(\mathbf{k}) = dk_xk_y$, $h_z(\mathbf{k}) = k_x^2/2 + (1-2d^2)k_y^2/2$, and $h_0(\mathbf{k}) = 0$. This Hamiltonian is obtained from the continuum Hamiltonian in Eq. (3) by a unitary transformation with $U = \frac{1-i\sigma_y}{\sqrt{2}}$.

We analyze the Landau levels of the continuum Hamiltonian with $\xi = 1$ after the replacement $k_x \rightarrow (a + a^{\dagger})/(\sqrt{2}l_B)$ and $k_y \rightarrow i(a - a^{\dagger})/(\sqrt{2}l_B)$, where $l_B = \sqrt{\hbar/eB}$ is a magnetic length, and a, a^{\dagger} are the annihilation and creation operators, respectively. To ensure the Hamiltonian's hermiticity, a symmetrization is performed: $k_xk_y = (k_x\hat{k}_y + \hat{k}_yk_x)/2 = i(a^2 - (a^{\dagger})^2)/(2l_B^2)$. Then, the continuum Hamiltonian in Eq. (A1) is transformed to

$$H_{LL} = \frac{1}{2l_B^2} = \begin{pmatrix} h_{11} & h_{12} \\ h_{21} & h_{22} \end{pmatrix}, \quad (\text{A2})$$

where

$$h_{11} = d_{\max}^2(a^2 + a^{\dagger 2}) + (1 - d_{\max}^2)(2a^{\dagger}a + 1), \quad (\text{A3})$$

$$h_{12} = d_{\max}(1 - \sqrt{1 - d_{\max}^2})a^2 - d_{\max}(1 + \sqrt{1 - d_{\max}^2})a^{\dagger 2} + d_{\max}\sqrt{1 - d_{\max}^2}(2a^{\dagger}a + 1) = h_{21}^{\dagger}, \quad (\text{A4})$$

$$h_{22} = -d_{\max}^2(a^2 + a^{\dagger 2}) - (1 - d_{\max}^2)(2a^{\dagger}a + 1). \quad (\text{A5})$$

Note that this Hamiltonian has a chiral symmetry $\{-\sigma_x, H_{LL}\} = -H_{LL}$, where $-\sigma_x = U^{-1}\sigma_zU$, when $d_{\max} = 0$ or $d_{\max} = 1$.

One can solve this problem using the following wavefunction:

$$|\psi\rangle = \sum_{n=0}^{\infty} v_n |u_n\rangle = \sum_{n=0}^{\infty} \begin{pmatrix} C_n \\ D_n \end{pmatrix} |u_n\rangle, \quad (\text{A6})$$

where $|u_n\rangle$ is a normalized state satisfying $a|u_n\rangle = \sqrt{n}|u_{n-1}\rangle$ and $a^{\dagger}|u_n\rangle = \sqrt{n+1}|u_{n+1}\rangle$, and C_n and D_n are complex coefficients. Using this wavefunction, the Hamiltonian in Eq. (A2) can be described as

$$H_{LL} = \frac{1}{2l_B^2} = \begin{pmatrix} h_0 & 0 & g_0 & 0 & \dots \\ 0 & h_1 & 0 & g_1 & \dots \\ g_0^{\dagger} & 0 & h_2 & 0 & \dots \\ 0 & g_1^{\dagger} & 0 & h_3 & \dots \\ \vdots & \vdots & \vdots & \vdots & \ddots \end{pmatrix}, \quad (\text{A7})$$

where

$$h_n = (2n + 1) \begin{pmatrix} 1 - d_{\max}^2 & d_{\max}\sqrt{1 - d_{\max}^2} \\ d_{\max}\sqrt{1 - d_{\max}^2} & -(1 - d_{\max}^2) \end{pmatrix}, \quad (\text{A8})$$

and

$$g_n = \sqrt{(n+1)(n+2)} \begin{pmatrix} d_{\max}^2 & d_{\max}(1 - \sqrt{1 - d_{\max}^2}) \\ -d_{\max}(1 + \sqrt{1 - d_{\max}^2}) & -d_{\max}^2 \end{pmatrix}. \quad (\text{A9})$$

From this Hamiltonian, one can get

$$\frac{1}{2l_B^2} \begin{pmatrix} h_n & g_n \\ g_n^{\dagger} & h_{n+2} \end{pmatrix} \begin{pmatrix} v_n \\ v_{n+2} \end{pmatrix} = E \begin{pmatrix} v_n \\ v_{n+2} \end{pmatrix}. \quad (\text{A10})$$

By using $v_{n+2} = [\tilde{E} - h_{n+2}]^{-1}g_n^{\dagger}v_n$, where $\tilde{E} = 2l_B^2E$, one can obtain the following equation:

$$\frac{1}{2l_B^2} [h_n + g_n(\tilde{E} - h_{n+2})^{-1}g_n^{\dagger}]v_n = Ev_n. \quad (\text{A11})$$

Since $n \leq 1$ this equation does not hold because n -th Landau level only comes from the $n + 2$ -th Landau levels and not from the $n - 2$ -th Landau levels. Thus, we consider the zero-th and first order energies separately. Calculating these, one can get the Landau levels in Eq (6) in the main text.

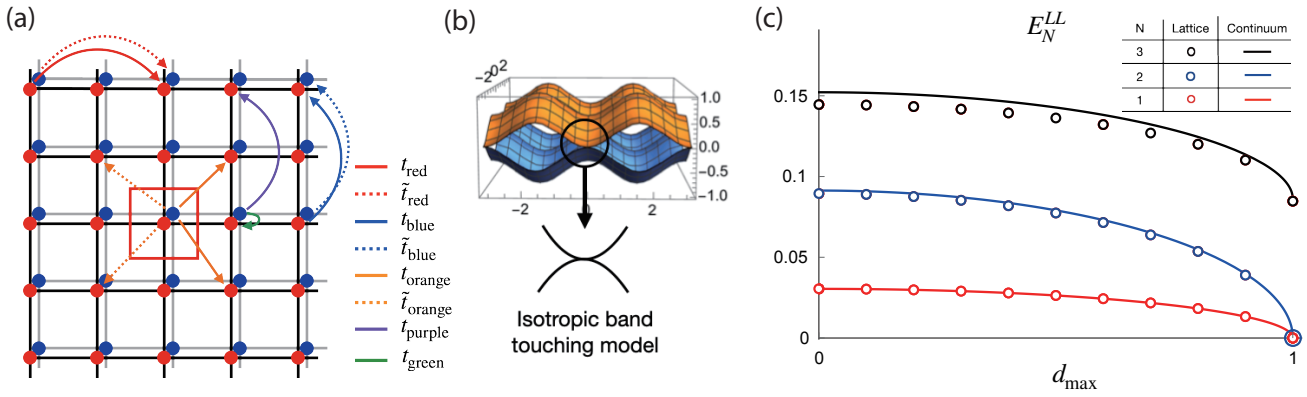


FIG. 4. (a) Lattice and hopping structure of the square lattice model. Here, t 's and \tilde{t} 's are the hopping parameters. In this model, d_{max} can be varied from 0 to 1 while maintaining the band structure by changing the hopping parameters. (b) Band structure of the lattice model. (c) Zero-th, first and second Landau levels of the lattice model and the continuum model in Eq (6) in the main text. The circles correspond to the lattice model, and the solid lines are from the continuum model.

Appendix B: Landau levels of a square lattice

To confirm our prediction based on a continuum model, we consider a lattice model on the square lattice whose effective Hamiltonian at the Γ point is given as Eq. (3) in the main text with $\xi = +1$. We consider various long-range hopping processes as illustrated in Fig. 4(a). The hopping parameters are given by $t_{\text{red}} = -\tilde{t}_{\text{red}} = -1/8$, $t_{\text{blue}} = -\tilde{t}_{\text{blue}} = -1/8 + d_{\text{max}}$, $t_{\text{orange}} = -\tilde{t}_{\text{orange}} = id_{\text{max}}/4$, $t_{\text{purple}} = -d_{\text{max}}\sqrt{1-d_{\text{max}}^2}/4$, and $t_{\text{green}} = d_{\text{max}}\sqrt{1-d_{\text{max}}^2}/2$. The explicit form of the tight-binding Hamiltonian for this model is

$$\begin{aligned}
 H_{\text{Lattice}} = \sum_{m,n} \frac{1-d_{\text{max}}^2}{2} & (A_{m,n}^\dagger A_{m,n} - B_{m,n}^\dagger B_{m,n}) + \left[t_{\text{green}} A_{m,n}^\dagger B_{m,n} + t_{\text{red}} (A_{m+2,n}^\dagger A_{m,n} - B_{m+2,n}^\dagger B_{m,n}) \right. \\
 & + t_{\text{blue}} (A_{m,n+2}^\dagger A_{m,n} - B_{m,n+2}^\dagger B_{m,n}) + t_{\text{purple}} (A_{m,n+2}^\dagger B_{m,n} + A_{m,n-2}^\dagger B_{m,n}) \\
 & \left. + t_{\text{orange}} (A_{m+1,n+1}^\dagger B_{m,n} + A_{m-1,n-1}^\dagger B_{m,n} - A_{m-1,n+1}^\dagger B_{m,n} - A_{m+1,n-1}^\dagger B_{m,n}) + h.c. \right]. \quad (\text{B1})
 \end{aligned}$$

The lattice Hamiltonian has the energy eigenvalues $E = \pm(2 - \cos 2k_x - \cos 2k_y)/4$, shown in Fig. 4(b), which remain invariant under changes in d_{max} ($0 \leq d_{\text{max}} \leq 1$).

Our predictions of Landau levels in Eq. (6) in the main text are confirmed by this lattice model. We consider commensurate magnetic fluxes ϕ satisfying $\phi/\phi_0 = 1/q$, where q is a natural number and ϕ_0 is the flux quantum. Figure 4(c) depicts the d_{max} -dependence of the zero-th, first, and second Landau levels. One can verify that our analytic results match well with the results of the lattice model.